

Article

Fresnel Lens Solar-Pumped Laser with Four Rods and Beam Merging Technique for Uniform and Stable Emission under Tracking Error Influence

Bruno D. Tibúrcio, Dawei Liang ^{*}, Joana Almeida, Dário Garcia, Miguel Catela, Hugo Costa and Cláudia R. Vistas

Centro de Física e Investigação Tecnológica, Departamento de Física, Faculdade de Ciências e Tecnologia, Universidade NOVA de Lisboa, Campus de Caparica, 2829-516 Caparica, Portugal; bdt12175@campus.fct.unl.pt (B.D.T.); jla@fct.unl.pt (J.A.); kongming.dario@gmail.com (D.G.); m.catela@campus.fct.unl.pt (M.C.)

* Correspondence: dl@fct.unl.pt

Abstract: Significant numerical improvements in Fresnel lens Nd:YAG solar laser collection efficiency, laser quality factors and tracking error compensation capacity by two Fresnel lenses as primary solar concentrators are reported here. A Nd:YAG four-rod side-pumping configuration was investigated. The four-rod side-pumping scheme consisted of two large aspherical lenses and four semi-cylindrical pump cavities, where the Nd:YAG laser rods were placed, enabling an efficient solar pumping of the laser crystals. A 104.4 W continuous-wave multimode solar laser power was achieved, corresponding to 29.7 W/m² collection efficiency, which is 1.68 times that of the most efficient experimental Nd:YAG side-pumped solar laser scheme with heliostat–parabolic mirror systems. End-side-pumped configuration has led to the most efficient multimode solar lasers, but it may cause more prejudicial thermal effects, poor beam quality factors and a lack of access to both rod end-faces to optimize the resonant cavity parameters. In the present work, an eight-folding-mirror laser beam merging technique was applied, aiming to attain one laser emission from the four laser rods that consist of the four-rod side-pumping scheme with a higher brightness figure of merit. A 79.8 W multimode laser output power was achieved with this arrangement, corresponding to 22.7 W/m². The brightness figure of merit was 0.14 W, being 1.6, 21.9 and 15.7 times that of previous experimental Nd:YAG solar lasers pumped by Fresnel lenses. A significant advance in tracking error tolerance was also numerically attained, leading to a 1.5 times enhancement in tracking error width at 10% laser power loss (TEW_{10%}) compared to previous experimental results.

Keywords: Fresnel lens; four-rod; solar pumping; beam merging; side-pumping; Nd:YAG



Citation: Tibúrcio, B.D.; Liang, D.; Almeida, J.; Garcia, D.; Catela, M.; Costa, H.; Vistas, C.R. Fresnel Lens Solar-Pumped Laser with Four Rods and Beam Merging Technique for Uniform and Stable Emission under Tracking Error Influence. *Energies* **2023**, *16*, 4815. <https://doi.org/10.3390/en16124815>

Academic Editor: Bin Yang

Received: 4 May 2023

Revised: 9 June 2023

Accepted: 16 June 2023

Published: 20 June 2023



Copyright: © 2023 by the authors. Licensee MDPI, Basel, Switzerland. This article is an open access article distributed under the terms and conditions of the Creative Commons Attribution (CC BY) license (<https://creativecommons.org/licenses/by/4.0/>).

1. Introduction

The conversion of solar radiation to laser light has the potential to enable laser applications in an almost low-carbon way, providing cost-effective laser radiation for high and average power applications and opening possibilities to numerous environmental and economic benefits in different technological segments. Solar-pumped lasers have already shown their feasibility for space and earth technologies [1–3], opening new prospects for solar energy technology [4]. Compared to electrical lasers, solar-pumped lasers offer possibilities to cut costs in the production of coherent optical radiation for laser applications. Additionally, solar-pumped lasers have possibilities for applications on Earth [5] and for material processing [6].

The first laser emission of 1 W pumped by the Sun was reported in 1966 [7]. Since then, other researchers further developed solar laser technology using heliostat–parabolic mirror systems (HPMS) to highly concentrate solar radiation onto the laser material [8–11]. Arashi et al. attained an 18 W solar laser emission with a Nd:YAG rod,

obtaining 1.4 W/m^2 collection efficiency [9]. Using compound parabolic concentrators, the collection efficiency achieved 6.7 W/m^2 [11]. A 37.2 W laser output was achieved using an HPMS by Liang et al., which raised the collection efficiency to 31.5 W/m^2 . In 2018, 32.50 W/m^2 was obtained using a Cr:Nd:YAG ceramic laser rod and an HPMS [12]. The current highest result obtained in multimode solar laser collection efficiency with an HPMS is 41.25 W/m^2 , with three Ce:Nd:YAG rods [13]. In 2023, 38.8 W/m^2 was obtained using Fresnel lens and Ce:Nd:YAG rods [14].

Important progress has been achieved by using Fresnel lenses for solar laser pumping [15–19]. Fresnel lenses can reduce weight, production cost and maintenance for solar concentration, despite presenting chromatic aberration [20]. Yabe et al. raised collection efficiency to 18.7 W/m^2 by pumping a Cr:Nd:YAG ceramic laser rod at the focus of a Fresnel lens [15]. A 19.3 W/m^2 collection efficiency was obtained in 2011 using a 0.64 m^2 Fresnel lens [16]. The collection efficiency was boosted to 30.0 W/m^2 by Dinh et al. in 2012, using a large area Fresnel lens [17] but with poor M^2 beam quality factors of 137:137 and beam brightness of 0.0064 W (the ratio between the laser output and the product of M_x^2 and M_y^2 quality factors [11]). Guan et al. obtained a 32.1 W/m^2 collection efficiency in 2018, with beam quality factors $M_x^2 = M_y^2 = 61$ and a brightness figure of merit of 0.0089 [21].

Different configurations like end-side-pumping [16,18,22–24] or side-pumping [9,10,19,25,26] have been studied. End-side-pumping arrangements reached the highest multimode solar laser outputs [12,16–19,22], while the current highest collection efficiency obtained side-pumping a Nd:YAG rod is 17.60 W/m^2 [27]. Side-pumping schemes have been studied for many years since this configuration may achieve higher laser beam brightness [11] due to the better distribution of the absorbed energy inside the laser medium. The detrimental thermal effects also become decreased, and both rod ends can be accessible to optimize laser resonator parameters and solar laser beam extraction. Regarding the tolerance to tracking errors, the side-pumping solar laser approach demonstrated the capability to compensate solar tracking errors in comparison to the end-side-pumping approaches [28,29]. A solar tracking system enables solar collectors to compensate for day and season changes observed in altitude and azimuth angles of the Sun. The efficiency of the solar pump absorption into the laser rod is critically influenced by solar tracking errors. Numerical studies have been carried out to improve the solar tracking error tolerance and overall emission stability of solar-pumped lasers [28,30–32] with HPMSs. The multi-rod schemes can also provide a significant alleviation of the thermal conditions of the laser medium. This helps increase the laser performance since each thinner laser rod will absorb less radiation compared to a single rod under the same solar pumping conditions, for which these detrimental thermal effects are much more pronounced, while also creating hot spots inside the laser material. The multi-rod solar laser demonstrated a much higher capability to compensate solar tracking errors in comparison to the single-rod approaches since the pump flux distribution can shift from one laser rod to another in a multi-rod scheme, being capable of maintaining a stable solar laser output power level [28,29]. In 2022, a Nd:YAG dual-rod side-pumping configuration was experimentally tested regarding its tracking error tolerance, achieving a $\text{TEW}_{10\%}$ (tracking error width at 10% laser power loss) of 0.6° in a horizontal side-pumping configuration and 1.4° in a vertical side-pumping configuration [33].

Due to the shaded zones between the reflected solar light and the focal common area in an HPMS, the collection efficiency of the solar laser emission decreases. Fresnel lenses have chromatic aberration, which also may reduce the collection efficiency, but not the stability and uniformity, of the solar laser emission. Therefore, research on solar lasers with Fresnel lenses offers the potential to avoid the above-mentioned constraints of HPMSs. Because they have a low weight and cost, are easy to maintain, can easily be mass-produced and prevent shaded zones, Fresnel lenses have been investigated in solar energy technology.

Here, we report significant advances in solar laser power, Nd:YAG side-pumping collection efficiency, laser beam quality factors, brightness figure of merit and tracking error

tolerance, using a Fresnel lens as a primary concentrator and two small folding mirrors to pump four laser rods in a side-pumping configuration. The solar laser head used two large aspherical silica lenses and four semi-cylindrical pump cavities, where four laser crystals were positioned, providing a further concentration onto the laser rods. The four-rod scheme obtained 104.4 W of laser power, leading to a 29.7 W/m^2 collection efficiency, being 1.68 times more than the highest result achieved with a Nd:YAG side-pumped arrangement by an HPMS [27]. This configuration led to the most efficient multimode solar laser output power, but it has more detrimental thermal induced effects and degraded beam quality factors due to the solar pump power not being uniformly absorbed inside the laser rods, which led to a lower brightness figure of merit, and limitations in the optimization procedure of the laser resonant cavity parameters. A single multimode solar laser beam was obtained from the four rods of the four-rod side-pumping solar laser head by using an eight-folding-mirror laser beam merging optical arrangement, and 79.8 W of multimode laser power was calculated with this technique. Additionally, a brightness figure of merit of 0.14 W was attained, being 1.6, 21.9 and 15.7 times more than that attained in previous experimental works using Nd:YAG rods pumped by Fresnel lenses, namely, Refs. [16,17,21], respectively. The tracking error compensation capacity of the Fresnel lens Nd:YAG side-pumping solar laser was also investigated. Relatively to the previous experimental dual-rod configuration studied using HPMS [33], with the same total tracking error of 0.57° and 0.03° in both azimuthal and altitude axes, respectively, the $\text{TEW}_{10\%}$ achieved by the present work was 0.9° , representing an advance in tracking error compensation capacity of 1.5 times, with no shading in the solar pumping and a more stable and uniform solar laser emission from each one of the individual rods. Furthermore, the collection efficiency was enhanced by 2.60 times compared to the 11.39 W/m^2 obtained in [33].

2. Fresnel Lens Nd:YAG Four-Rod Solar Laser System

2.1. Fresnel Lens Solar Concentration System

The collection and the concentration of solar energy can be attained using low-cost, lightweight, easily available and easily mass-produced Fresnel lenses built of polymethyl methacrylate material, albeit having inherent chromatic aberration. The primary solar concentration system of this work consisted of two parallel Fresnel lenses (1.5 m diameter; focal length of 2.39 m), with a 3.53 m^2 effective collection area, concentrating the solar radiation towards two stationary small folding mirrors of 0.3 m^2 each, which were 1.0 m apart from the solar laser head to redirect the solar radiation, as depicted in Figure 1.

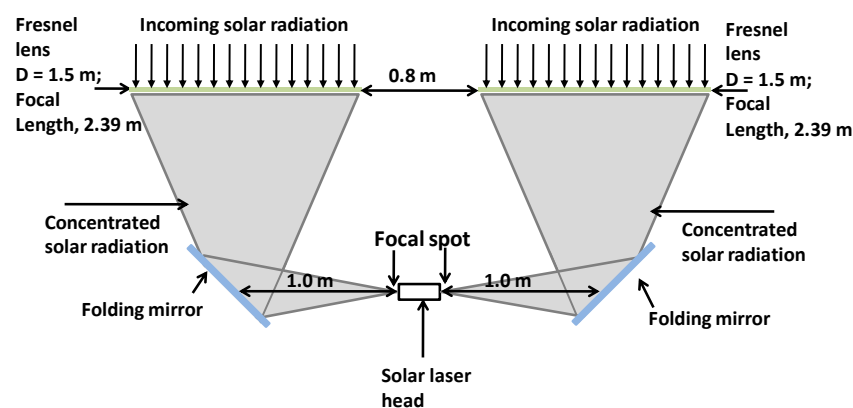


Figure 1. Schematics of the Fresnel lens solar concentration system. The two stationary small folding mirrors are 1.0 m apart from the solar laser head with areas of 0.3 m^2 each.

The Fresnel lens system presented no shaded zones due to the supporting mechanics being HPMSs. A 1767 W solar power could be concentrated by each Fresnel lens into a common focal spot, considering 1000 W/m^2 of solar irradiance.

2.2. Four-Rod Solar Laser Side-Pumping Scheme

Figure 2a–c depicts the four-rod side-pumping scheme used in this work, which consisted of two fused silica aspherical lenses and four semi-cylindrical pump cavities, where the four 4.0 mm diameter and 30 mm length laser crystals were positioned. All the key dimensions of the scheme are indicated in the figure. The aspherical lenses had a 58 mm radius of curvature, a 116 mm diameter and a -1 conic factor. Each one of the four pump cavities had a 20 mm \times 21 mm rectangular input aperture and a 14.8 mm \times 21 mm output aperture. The four semi-cylindrical pump cavities had a 6.0 mm radius, 21 mm length and 3.55 mm height. For the pump cavity mirrors, 98% reflectivity was considered. Four resonant cavities were set for the laser power extraction of the four-rod scheme and were composed of one high reflector at the 1064 nm end mirror with 99.9% reflectivity and one partial reflector at the 1064 nm output mirror with 95% reflectivity.

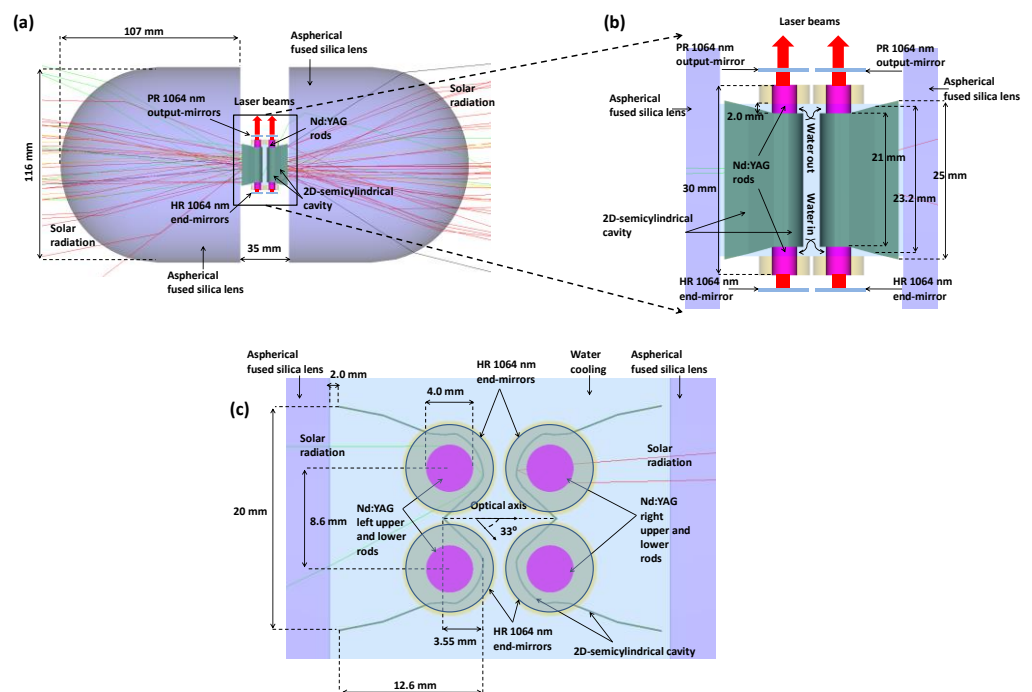


Figure 2. Schematics of the four-rod solar laser scheme, with its key dimensions indicated: (a) side-view with the aspherical lenses and the resonant laser cavities; (b) side-view with key dimensions and resonant laser cavities; (c) front view with key dimensions.

3. Numerical Analysis of the Nd:YAG Four-Rod Solar Laser

3.1. Ray Tracing Performance of the Nd:YAG Four-Rod Solar Laser

Non-sequential ray-tracing Zemax[®] software (<https://www.zemax.com/>) was used to optimize the solar laser scheme. A 1000 W/m² solar irradiance was taken into account in the simulations. The peak absorption and the respective absorption coefficients were added in ZEMAX[®] [16,19,22]. The central wavelengths used for these peaks were 527 nm, 531 nm, 568 nm, 578 nm, 586 nm, 592 nm, 732 nm, 736 nm, 743 nm, 746 nm, 753 nm, 758 nm, 790 nm, 793 nm, 803 nm, 805 nm, 808 nm, 811 nm, 815 nm, 820 nm, 865 nm and 880 nm. The 22 peak absorption wavelengths and their spectral irradiance (W/m²/nm) were consulted and integrated in the software calculations [34]. The absorption spectrum of all the materials was introduced in the software as numerical input data.

The effective absorption coefficient was taken into account, and summing up the absorbed pump radiation of all the zones in which the laser rod was divided (18,000 zones), the absorption of the solar pump flux of the laser rod was computed. The overlap between the Nd:YAG material absorption spectrum and the solar spectrum was considered [35]. The absorbed pump flux distribution of the four-rod scheme, with four 4.0 mm diameter and 30 mm length rods, is shown in Figure 3.

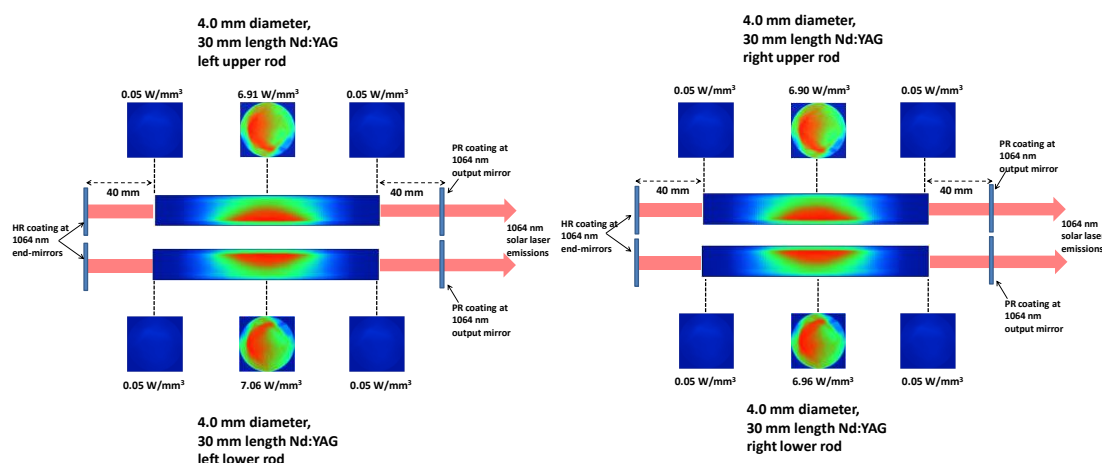


Figure 3. The absorbed pump flux distributions of the 4.0 mm diameter and 30 mm length rods of the four-rod scheme. Red color means maximum pump absorption, and blue means little or no absorption.

The non-uniform pump flux absorption profiles significantly affected the laser beam profile and, hence, the laser beam quality factors. In Section 6, the laser beam merging technique is presented to mitigate this issue, using an eight-folding-mirror optical arrangement, not only to provide one single laser beam from the four rods but also to compensate those non-uniformities in the pump flux absorption profiles, allowing a significant improvement in the beam quality factors of this single laser emission, largely increasing its brightness figure of merit compared to each individual solar laser emission with those non-uniformities.

The numerical data corresponding to the absorbed pump flux distributions of the four-rod scheme was integrated in the LASCADTM software (<https://www.las-cad.com/>) for the optimization of the laser resonant cavity and the extraction of the laser output power.

3.2. LASCADTM Laser Output from the Four-Rod Solar Laser

The resonant cavity analysis was optimized with LASCADTM software. The Nd:YAG medium shows interesting properties in comparison to other laser media [36], adding robustness to the solar laser. The fluorescence lifetime of 230 μs and the absorption and scattering losses of the 0.003 cm^{-1} and $2.8 \times 10^{-19}\text{ cm}^2$ stimulated cross-section for the 1.0 at% Nd:YAG laser medium were included in the LASCADTM simulations, as well as the solar pump wavelength of 660 nm (mean absorbed and intensity-weighted) [26]. Optical imperfections for the 1064 nm mirrors, such as the optical coating losses of 0.2% and 0.1% for the anti-reflection coatings of the laser rods and the HR coatings of the end mirrors, respectively, were also included in the simulations.

The dimensions of the laser crystals, as well as the reflectivities of the mirrors in the symmetrical laser resonant cavities, were optimized for multimode laser power extractions, as shown in Figure 4. The scheme was optimized using 110 mm for the length resonant cavity and a radius-of-curvature of -10 m for the output and the end mirrors. The laser power obtained from the optimization process was 104.4 W, with 26.1 W from each of the four rods, and the laser beam quality factors were $M_x^2 = M_y^2 = 48$.

The rod diameter significantly influences the output power because of the optimum mode match between the laser beam waist radius and the pump mode [37]. Figure 5 shows the laser output attained with incoming solar light. The slope efficiency obtained is also shown, as well as each individual rod of the scheme.

With the non-sequential ray-tracing simulation, the interaction of light with all the solar laser components (Fresnel lens, aspheric silica lens, pump cavity and laser rods) were taken into account in Zemax[®], as described in Section 3.1. Then, the numerical data corresponding to the absorbed pump flux distributions of the rods were exported to

LASCADTM software, and the laser output power was numerically calculated, taking into account the optical imperfections of the output mirrors in the resonant cavity.

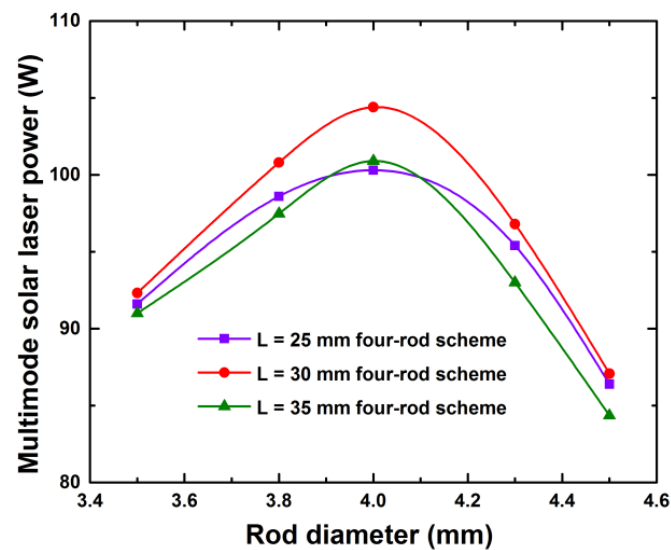


Figure 4. Total solar laser power numerically calculated, as a function of the rod diameter and length (L), for the Nd:YAG four-rod scheme.

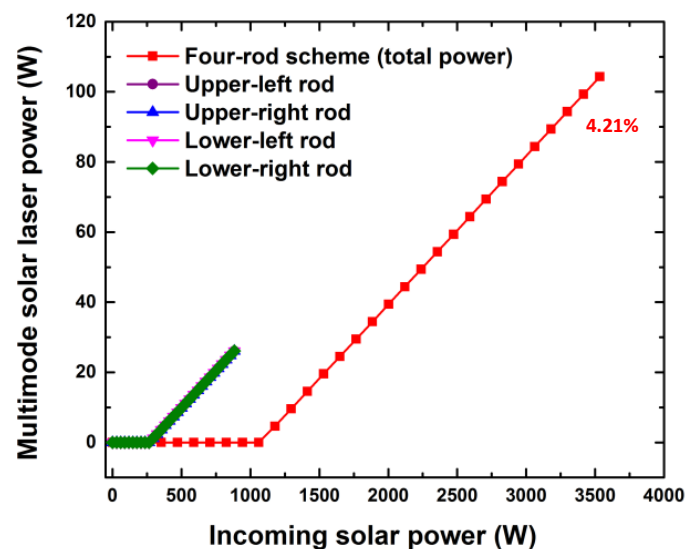


Figure 5. Solar laser output power numerically calculated from the four rods summed up, as a function of the incoming solar light. Each individual laser crystal and the slope efficiency are also represented.

Figure 6 shows the laser beam pattern numerically obtained from one laser crystal of the four-rod scheme. For laser emission near the threshold, a low-order laser beam appears. With the increase in input solar pump power, a multimode laser beam profile, as shown in Figure 6, finally emerges.

The threshold pump power numerically computed was 265 W for each one of the rods of the four-rod scheme, which resulted in a 1060 W threshold pump power with four crystals emitting. The slope efficiency obtained was 4.21%. Table 1 below summarizes the results obtained.

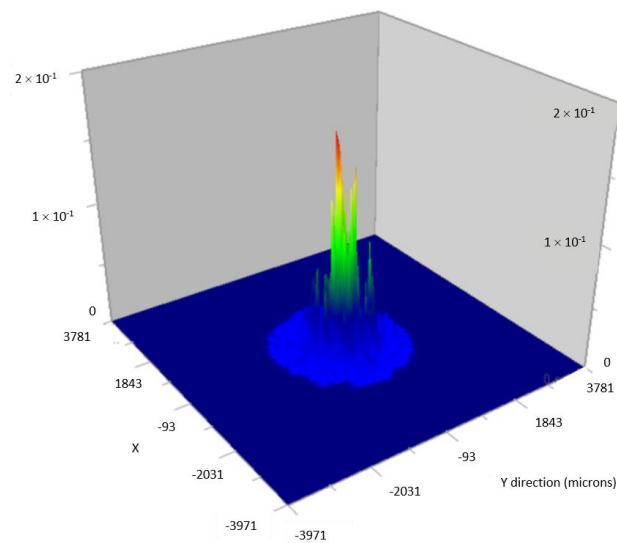


Figure 6. Solar laser beam pattern numerically calculated from one laser rod of the four-rod scheme by LASCAD™ software.

Table 1. Laser power, collection efficiency, slope efficiency and threshold pump power for the Nd:YAG four-rod solar laser.

Scheme	Parameter			
	Laser Output Power (W)	Collection Efficiency (W/m ²)	Slope Efficiency (%)	Threshold Pump Power (W)
Nd:YAG four-rod side-pumping scheme	104.4	29.7	4.21	1060

4. Fresnel Lens Four-Rod Thermal Performance Analysis

In this work, the thermal condition of the Nd:YAG rod under solar pumping was studied by integrating the absorption of the pump power input data from Zemax® software into LASCAD™ software. The heat load, temperature and stress intensity of the material were determined for one rod of the scheme. Figure 7 below summarizes the results.

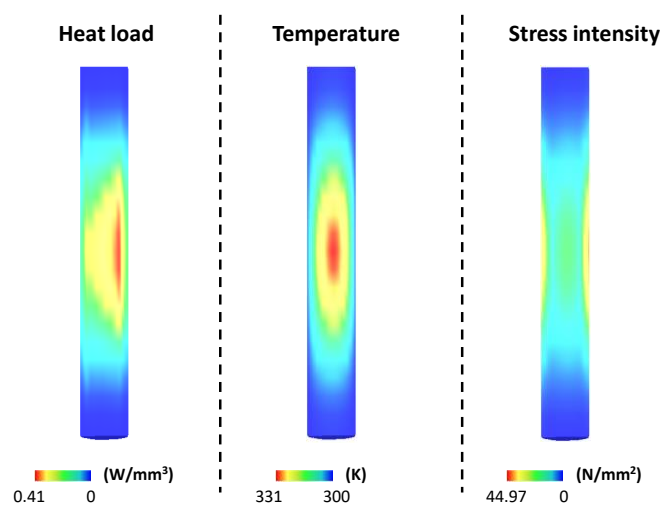


Figure 7. Heat load, temperature and stress intensity for the 4.0 mm diameter and 30 mm length rod from the four-rod solar laser.

For each of the rods of the four-rod solar laser, the heat load calculated was 0.41 W/mm³. A temperature of 331 K and a stress intensity of 44.95 N/mm² were numerically achieved.

5. Nd:YAG Four-Rod Scheme Solar Laser with Fresnel Lenses under Tracking Error Influence

The solar tracking errors displaces the focus from its optimal alignment, which causes losses in the collection efficiency [38,39]. In order to attain high efficiencies in solar concentration with point-focusing concentrators, it is mandatory to use a solar tracking system to compensate for day and season variations observed in the altitude and azimuth angles of the Sun, usually with an angle less than 0.05° [40–42].

The performance under tracking error influence of the Fresnel lens four-rod scheme was investigated and compared with the horizontal scheme from [33], for which experimental results were influenced by the inherent shaded zones at the focus of the HPMS. Tracking errors up to 0.57° to 0.03° in the azimuthal and altitude axes, respectively, studied experimentally [33], were numerically investigated in this work.

The normalized total laser output, as a function of the total tracking error in altitude and azimuth directions simultaneously, for the four-rod side-pumping scheme studied in this work and the previous dual-rod scheme from [33] is shown in Figure 8. Each laser rod of both schemes is also represented. The solar laser output powers from the four rods were measured in LASCADTM software, with the same pumping and laser resonant conditions. Solar tracking errors were introduced in the solar source of the optical model for both azimuth (xx axis) and altitude (yy axis) axes, simultaneously. The four-rod from this work obtained 0.9° TEW_{10%}, while the previous dual-rod from [33] attained 0.6° TEW_{10%}. This parameter was determined from the total solar laser output power obtained from the four rods with the optimum alignment (no tracking errors) and compared to the solar laser output power obtained by simulating the four-rod scheme with tracking errors in the solar source, thus calculating the corresponding laser output power for each value of solar tracking error used. It is also observable in the experimental results from [33] that the lower rod of the dual-rod presents a sharp decrease in its laser output power, relatively to the upper rod, which remains more stable, due to the inherent shading of an HPMS. By using Fresnel lenses as primary concentrators, this shading effect is prevented. Regarding the numerical results in [31,32], those results were attained in heliostat–parabolic mirror systems without the shading represented in the numerical results.

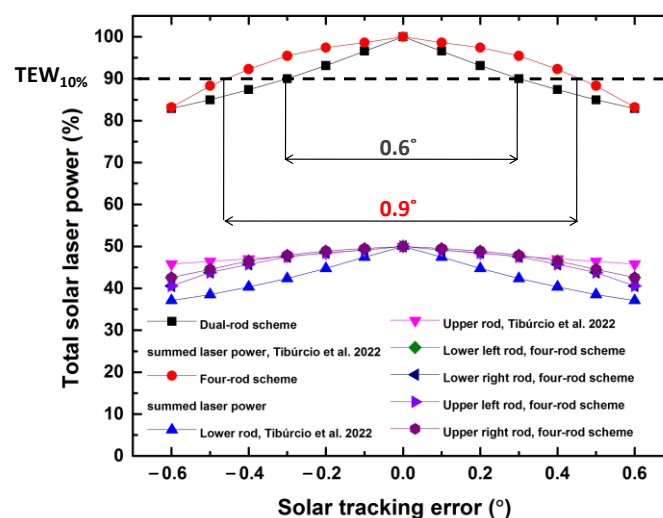


Figure 8. Normalized summed laser output, as a function of the total solar tracking error in altitude and azimuth directions simultaneously, for the four-rod and the dual-rod from Tibúrcio et al. [33]. The performance from each rod from both schemes is also represented.

Four-rod side-pumping using a Fresnel lens is an interesting alternative to obtain a tracking-error-compensated solar-pumped laser, in addition to providing large laser output powers.

6. Fresnel Lens Four-Rod Scheme with Beam Merging Technique

The beam merging technique was applied to provide only one laser beam emitted from the four rods of the four-rod scheme. The set up of eight HR 1064 nm folding mirrors $M_0, M_1, M_2, M_3, M_4, M_5, M_6$ and M_7 , one HR 1064 nm end-mirror and a PR 1064 nm output mirror composed the resonant cavity, together with the four laser rods, as shown in Figure 9a,b. Each laser crystal of the four-rod scheme was divided into two sections: one representing the regions with higher flux absorption (A and B), indicated by red arrows, and the other representing the regions with lower flux absorption (A' and B'), indicated by pink arrows. The representation of the laser beam, passing back and forth through those regions of the crystals, were also divided in two in order to represent the contributions of each one of these pumped regions to the total solar laser emission. A compensation of the laser beam profile could be obtained with this optical arrangement, in which the parts of the laser beams passing through the regions of the laser crystals with higher pump flux absorptions (A and B) were folded to the regions of the laser crystals with lower pump flux absorptions (A' and B'). A 79.8 W multimode laser power was attained with this configuration, allowing the emission of one single laser beam from the four rods with beam quality factors of $M_x^2 = M_y^2 = 24$ and a higher brightness figure of merit of 0.14 W, compared to the emission of each individual rod, which attained 0.04 W.

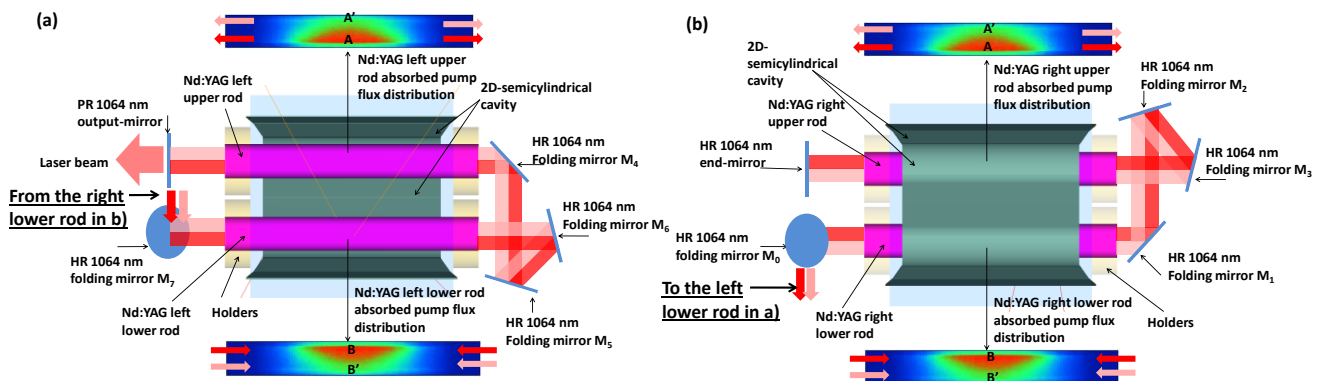


Figure 9. Laser beam merging design for the four-rod scheme, providing only one laser beam emitted from the four rods: (a) left upper and lower rods; (b) right upper and lower rods. Eight HR 1064 nm folding mirrors ($M_0, M_1, M_2, M_3, M_4, M_5, M_6$ and M_7) were used. The red arrows indicate the zones of the crystals with higher flux absorption, while the pink arrows indicate the zones of the crystals with lower flux absorption.

7. Discussions

Table 2 provides the comparison of the four-rod scheme and the results of the solar laser using Fresnel lenses in end-side pumping arrangements.

Table 2. Solar laser power, collection efficiency, M^2 quality factors and the brightness figure of merit for the four-rod solar laser emitting four beams and the four-rod solar laser emitting one beam compared to results of Nd:YAG solar-pumped lasers using Fresnel lenses in end-side pumping configurations.

Parameters	References			Present Numerical Work	
	Liang et al. [16], End-Side-Pumping Configuration	Dinh et al. [17], End-Side-Pumping Configuration	Guan et al. [21] End-Side-Pumping Configuration	Four-Rod Side-Pumping Scheme with Four Laser Beams	Four-Rod Side-Pumping Scheme with One Laser Beam
Laser output power (W)	9.7	120	33.1	104.4	79.8
Collection efficiency (W/m^2)	19.3	30	32.1	29.7	22.7
M^2 factors ($M_x^2 = M_y^2$)	10.6	137	61	48	24
Brightness figure of merit (W)	0.086	0.0064	0.0089	0.04	0.14

The Nd:YAG four-rod side-pumping scheme attained 104.4 W of solar laser output power, which corresponds to a $29.7 W/m^2$ collection efficiency, being 1.68 times that of previous results obtained using a single Nd:YAG rod in a side-pumping scheme [27]. This

value is slightly lower in comparison with the previous experimental works by Liang et al. [16], Dinh et al. [17] and Guan et al. [21] using Fresnel lenses in end-side pumping schemes, which reached the highest results in the multimode solar laser emission. The multi-rod side-pumping scheme presents important advantages, such as the diminishing of the detrimental thermal induced effects due to the better distribution of the pump flux absorption by the crystals, the potential to improve the quality factors and brightness, and an improved tracking error capacity.

8. Conclusions

A Nd:YAG four-rod side-pumping scheme was numerically studied in this work. The first stage was composed of two Fresnel lenses of 1.5 m diameter and two small folding mirrors as primary concentrators. The second stage had two aspherical lenses, and the third stage had four semi-cylindrical pumping cavities, where four 4.0 mm diameter and 30 mm length laser crystals were set and pumped at the focus of each one of the Fresnel lenses. The Fresnel lenses, the solar laser head and the resonant cavity were optimized using Zemax[®] and LASCAD[™] software. Numerical calculations were performed in order to calculate laser power, its threshold regarding the absorption of the pump power and its slope efficiency.

An eight-folding-mirror beam merging technique was applied in order to achieve one multimode solar laser emission from the four-rod side-pumping scheme with laser beam quality factors of $M_x^2 = M_y^2 = 24$, leading to a brightness figure of merit of 0.14 W, which is 1.6, 21.9 and 15.7 times more than that reported in previous works with Nd:YAG rods pumped by Fresnel lens systems, namely, Refs. [16,17,21], respectively.

The Fresnel lens Nd:YAG four-rod scheme was investigated under tracking error influence and compared to that of the previous dual-rod experimentally investigated by an HPMS in [33]. The present work has shown an advancement in tracking error compensation capacity of 1.5 times while preventing the inherent shading effect from the HPMS, showing important advantages in the stability and uniformity of the solar laser emission.

The present work with four Nd:YAG rods in a side-pumping configuration ensured an improvement in the beam quality factors and the brightness figure of merit while obtaining large laser output powers, which is useful for many applications in a low-carbon way.

Author Contributions: Conceptualization, B.D.T. and D.L.; methodology, B.D.T., D.L. and J.A.; software, B.D.T., D.G. and M.C.; validation, B.D.T., D.L., J.A. and D.G.; formal analysis, B.D.T., D.L. and J.A.; investigation, B.D.T., D.L., J.A., D.G., M.C., H.C. and C.R.V.; resources, D.L. and J.A.; data curation, B.D.T., D.G. and M.C.; writing—original draft preparation, B.D.T. and D.L.; writing—review and editing, B.D.T., D.L., J.A., M.C., H.C., D.G. and C.R.V.; supervision, D.L.; project administration, D.L.; funding acquisition, D.L. and J.A. All authors have read and agreed to the published version of the manuscript.

Funding: This research was funded by the Science and Technology Foundation of Portuguese Ministry of Science, Technology and Higher Education (FCT-MCTES), via the strategic project UIDB/00068/2020 and the exploratory research project EXPL/FIS-OTI/0332/2021.

Data Availability Statement: Not applicable.

Acknowledgments: The FCT-MCTES fellowship grants SFRH/BPD/125116/2016, PD/BD/142827/2018, SFRH/BD/145322/2019, 2021.06172.BD and CEECIND/03081/2017 of Cláudia R. Vistas, Dário Garcia, Miguel Catela, Hugo Costa and Joana Almeida, respectively, are acknowledged.

Conflicts of Interest: The authors declare no conflict of interest.

References

1. Overton, G. *NOVEL LASERS: “Solar-Pumped Nd:YAG Lasers Getting Brighter”*; Laser Focus World: Nashua, NH, USA, 2013.
2. Lando, M.; Shimony, Y.; Benmair, R.M.J.; Abramovich, D.; Krupkin, V.; Yogev, A. Visible solar-pumped lasers. *Opt. Mater.* **1999**, *13*, 111–115. [[CrossRef](#)]
3. Takashi, Y.; Tomomasa, O.; Hung, D.T.; Hiroki, K.; Junichi, N.; Kouta, O. Demonstration of Solar-Pumped Laser-Induced Magnesium Production from Magnesium Oxide. *Magnes. Technol.* **2012**, *2012*, 55–58. [[CrossRef](#)]

4. Graham-Rowe, D. Solar-powered lasers. *Nat. Photonics* **2010**, *4*, 64–65. [[CrossRef](#)]
5. Motohiro, T.; Takeda, Y.; Ito, H.; Hasegawa, K.; Ikesue, A.; Ichikawa, T.; Higuchi, K.; Ichiki, A.; Mizuno, S.; Ito, T.; et al. Concept of the solar-pumped laser-photovoltaics combined system and its application to laser beam power feeding to electric vehicles. *Jpn. J. Appl. Phys.* **2017**, *56*, 08MA07. [[CrossRef](#)]
6. Yabe, T.; Uchida, S.; Ikuta, K.; Yoshida, K.; Baasandash, C.; Mohamed, M.S.; Sakurai, Y.; Ogata, Y.; Tuji, M.; Mori, Y.; et al. Demonstrated fossil-fuel-free energy cycle using magnesium and laser. *Appl. Phys. Lett.* **2006**, *89*, 261107. [[CrossRef](#)]
7. Young, C.G. A Sun-Pumped cw One-Watt Laser. *Appl. Opt.* **1966**, *5*, 993–997. [[CrossRef](#)]
8. Weksler, M.; Shwartz, J. *Solar Pumped Solid State Lasers*; SPIE: Bellingham, WA, USA, 1987; Volume 0736.
9. Arashi, H.; Oka, Y.; Sasahara, N.; Kaimai, A.; Ishigame, M. A Solar-Pumped cw 18 W Nd:YAG Laser. *Jpn. J. Appl. Phys.* **1984**, *23*, 1051–1053. [[CrossRef](#)]
10. Benmair, R.M.J.; Kagan, J.; Kalisky, Y.; Noter, Y.; Oron, M.; Shimony, Y.; Yogev, A. Solar-pumped Er,Tm,Ho:YAG laser. *Opt. Lett.* **1990**, *15*, 36–38. [[CrossRef](#)]
11. Lando, M.; Kagan, J.; Linyekin, B.; Dobrusin, V. A solar-pumped Nd:YAG laser in the high collection efficiency regime. *Opt. Commun.* **2003**, *222*, 371–381. [[CrossRef](#)]
12. Liang, D.; Vistas, C.R.; Tibúrcio, B.D.; Almeida, J. Solar-pumped Cr:Nd:YAG ceramic laser with 6.7% slope efficiency. *Sol. Energy Mater. Sol. Cells* **2018**, *185*, 75–79. [[CrossRef](#)]
13. Liang, D.; Vistas, C.R.; Garcia, D.; Tibúrcio, B.D.; Catela, M.; Costa, H.; Guillot, E.; Almeida, J. Most efficient simultaneous solar laser emissions from three Ce:Nd:YAG rods within a single pump cavity. *Sol. Energy Mater. Sol. Cells* **2022**, *246*, 111921. [[CrossRef](#)]
14. Cai, Z.; Zhao, C.; Zhao, Z.; Zhang, J.; Zhang, Z.; Zhang, H. Efficient 38.8 W/m² solar pumped laser with a Ce:Nd:YAG crystal and a Fresnel lens. *Opt. Express* **2023**, *31*, 1340–1353. [[CrossRef](#)]
15. Yabe, T.; Ohkubo, T.; Uchida, S.; Yoshida, K.; Nakatsuka, M.; Funatsu, T.; Mabuti, A.; Oyama, A.; Nakagawa, K.; Oishi, T.; et al. High-efficiency and economical solar-energy-pumped laser with Fresnel lens and chromium codoped laser medium. *Appl. Phys. Lett.* **2007**, *90*, 261120. [[CrossRef](#)]
16. Liang, D.; Almeida, J. Highly efficient solar-pumped Nd:YAG laser. *Opt. Express* **2011**, *19*, 26399–26405. [[CrossRef](#)]
17. Dinh, T.H.; Ohkubo, T.; Yabe, T.; Kuboyama, H. 120 watt continuous wave solar-pumped laser with a liquid light-guide lens and an Nd:YAG rod. *Opt. Lett.* **2012**, *37*, 2670–2672. [[CrossRef](#)]
18. Xu, P.; Yang, S.; Zhao, C.; Guan, Z.; Wang, H.; Zhang, Y.; Zhang, H.; He, T. High-efficiency solar-pumped laser with a grooved Nd:YAG rod. *Appl. Opt.* **2014**, *53*, 3941–3944. [[CrossRef](#)]
19. Liang, D.; Almeida, J. Solar-Pumped TEM₀₀-mode Nd:YAG laser. *Opt. Express* **2013**, *21*, 25107–25112. [[CrossRef](#)]
20. Jing, L.; Liu, H.; Wang, Y.; Xu, W.; Zhang, H.; Lu, Z. Design and Optimization of Fresnel Lens for High Concentration Photovoltaic System. *Int. J. Photoenergy* **2014**, *2014*, 7. [[CrossRef](#)]
21. Guan, Z.; Zhao, C.; Li, J.; He, D.; Zhang, H. 32.1 W/m² continuous wave solar-pumped laser with a bonding Nd:YAG/YAG rod and a Fresnel lens. *Opt. Laser Technol.* **2018**, *107*, 158–161. [[CrossRef](#)]
22. Liang, D.; Almeida, J.; Vistas, C.R.; Guillot, E. Solar-pumped Nd:YAG laser with 31.5 W/m² multimode and 7.9 W/m² TEM₀₀-mode collection efficiencies. *Sol. Energy Mater. Sol. Cells* **2017**, *159*, 435–439. [[CrossRef](#)]
23. Almeida, J.; Liang, D.; Vistas, C.R.; Guillot, E. Highly efficient end-side-pumped Nd:YAG solar laser by a heliostat-parabolic mirror system. *Appl. Opt.* **2015**, *54*, 1970–1977. [[CrossRef](#)] [[PubMed](#)]
24. Almeida, J.; Liang, D.; Guillot, E.; Abdel-Hadi, Y. A 40 W cw Nd:YAG solar laser pumped through a heliostat: A parabolic mirror system. *Laser Phys.* **2013**, *23*, 6. [[CrossRef](#)]
25. Liang, D.; Almeida, J.; Guillot, E. Side-pumped continuous-wave Cr:Nd:YAG ceramic solar laser. *Appl. Phys. B-Lasers Opt.* **2013**, *111*, 305–311. [[CrossRef](#)]
26. Weksler, M.; Shwartz, J. Solar-pumped solid-state lasers. *IEEE J. Quantum Electron.* **1988**, *24*, 1222–1228. [[CrossRef](#)]
27. Liang, D.; Vistas, C.R.; Almeida, J.; Tibúrcio, B.D.; Garcia, D. Side-pumped continuous-wave Nd:YAG solar laser with 5.4% slope efficiency. *Sol. Energy Mater. Sol. Cells* **2019**, *192*, 147–153. [[CrossRef](#)]
28. Tibúrcio, B.D.; Liang, D.; Almeida, J.; Garcia, D.; Vistas, C.R.; Morais, P.J. Highly efficient side-pumped solar laser with enhanced tracking-error compensation capacity. *Opt. Commun.* **2020**, *460*, 125156. [[CrossRef](#)]
29. Tibúrcio, B.D.; Liang, D.; Almeida, J.; Garcia, D.; Vistas, C.R. Dual-rod pumping approach for tracking error compensation in solar-pumped lasers. *J. Photonics Energy* **2019**, *9*, 028001. [[CrossRef](#)]
30. Tibúrcio, B.D.; Liang, D.; Almeida, J.; Garcia, D.; Catela, M.; Costa, H.; Vistas, C.R. Improving side-pumped solar lasers using ring-array concentrators. *Int. J. Sustain. Energy* **2021**, *41*, 868–888. [[CrossRef](#)]
31. Catela, M.; Liang, D.; Vistas, C.R.; Garcia, D.; Costa, H.; Tibúrcio, B.D.; Almeida, J. Highly Efficient Four-Rod Pumping Approach for the Most Stable Solar Laser Emission. *Micromachines* **2022**, *13*, 1670. [[CrossRef](#)]
32. Costa, H.; Liang, D.; Almeida, J.; Catela, M.; Garcia, D.; Tibúrcio, B.D.; Vistas, C.R. Seven-Rod Pumping Concept for Highly Stable Solar Laser Emission. *Energies* **2022**, *15*, 9140. [[CrossRef](#)]
33. Tibúrcio, B.D.; Liang, D.; Almeida, J.; Garcia, D.; Catela, M.; Costa, H.; Vistas, C.R. Tracking error compensation capacity measurement of a dual-rod side-pumping solar laser. *Renew. Energy* **2022**, *195*, 1253–1261. [[CrossRef](#)]
34. ASTM G173-03; Standard Tables for Reference Solar Spectral Irradiances: Direct Normal and Hemispherical on 37° Tilted Surface. International: West Conshohocken, PA, USA, 2012.

35. Bin, Z.; Changming, Z.; Jianwei, H.; Yang, S. The study of active medium for solar-pumped solid-state lasers. *Acta Opt. Sin.* **2007**, *27*, 1797–1801.
36. Koechner, W. *Solid-State Laser Engineering*, 6th ed.; Springer: New York, NY, USA, 2006; Volume 1.
37. Huang, Z. Theoretical optimization of output power in side pumped Nd³⁺:YAG solar laser. *Opt. Laser Technol.* **2019**, *111*, 592–596. [[CrossRef](#)]
38. Rabl, A. *Active Solar Collectors and Their Applications*; Oxford University Press: New York, NY, USA, 1985; Volume 1, p. 523.
39. Kalogirou, S. *Solar Energy Engineering*, 2nd ed.; Academic Press: Cambridge, MA, USA, 2013; Volume 1, p. 840.
40. Reda, I.; Andreas, A. Solar position algorithm for solar radiation applications. *Sol. Energy* **2004**, *76*, 577–589. [[CrossRef](#)]
41. Aiuchi, K.; Yoshida, K.; Katayama, Y.; Nakamura, M.; Nakamura, K. Sun Tracking Photo-Sensor for Solar Thermal Concentrating System. *Int. Sol. Energy Conf.* **2004**, *27475*, 625–631.
42. Abdallah, S.; Nijmeh, S. Two axes sun tracking system with PLC control. *Energy Convers. Manag.* **2004**, *45*, 1931–1939. [[CrossRef](#)]

Disclaimer/Publisher’s Note: The statements, opinions and data contained in all publications are solely those of the individual author(s) and contributor(s) and not of MDPI and/or the editor(s). MDPI and/or the editor(s) disclaim responsibility for any injury to people or property resulting from any ideas, methods, instructions or products referred to in the content.